COMMUNICATIONS CHEMISTRY

ARTICLE

https://doi.org/10.1038/s42004-020-00336-7 OPEN

pK_a of the ligand water molecules in the oxygen-evolving Mn_4CaO_5 cluster in photosystem II

Keisuke Saito [1,2], Minesato Nakagawa[1] & Hiroshi Ishikita [1,2]✉

Release of the protons from the substrate water molecules is prerequisite for O_2 evolution in photosystem II (PSII). Proton-releasing water molecules with low pK_a values at the catalytic moiety can be the substrate water molecules. In some studies, one of the ligand water molecules, W2, is regarded as OH^-. However, the PSII crystal structure shows neither proton acceptor nor proton-transfer pathway for W2, which is not consistent with the assumption of W2 = OH^-. Here we report the pK_a values of the four ligand water molecules, W1 and W2 at Mn4 and W3 and W4 at Ca^{2+}, of the Mn_4CaO_5 cluster. pK_a(W1) ≈ pK_a(W2) << pK_a(W3) ≈ pK_a(W4) in the Mn_4CaO_5 cluster in water. However, pK_a(W1) ≈ pK_a(D1-Asp61) << pK_a(W2) in the PSII protein environment. These results suggest that in PSII, deprotonation of W2 is energetically disfavored as far as W1 exists.

[1] Department of Applied Chemistry, The University of Tokyo, 7-3-1 Hongo, Bunkyo-ku, Tokyo 113-8654, Japan. [2] Research Center for Advanced Science and Technology, The University of Tokyo, 4-6-1 Komaba, Meguro-ku, Tokyo 153-8904, Japan. ✉email: hiro@appchem.t.u-tokyo.ac.jp

In the water-splitting enzyme, photosystem II (PSII), oxygen evolution proceeds, removing four protons (H^+) and four electrons from two substrate water molecules at the oxygen-evolving complex, Mn_4CaO_5 (Fig. 1)[1,2]. The Mn_4CaO_5 cluster has two ligand water molecules, W1 and W2, at the dangling Mn4 site and another two ligand water molecules, W3 and W4, at the Ca^{2+} site. These bound water molecules are candidates as potential substrates for water oxidation. As electron transfer occurs, the oxidation state of the oxygen-evolving complex, S_n, increases. Release of protons is observed with the typical stoichiometry of 1:0:1:2 for $S_0 \rightarrow S_1 \rightarrow S_2 \rightarrow S_3 \rightarrow S_0$, and O_2 is evolved in the S_3 to S_0 transition. After O_2 evolution, the first proton-releasing step is the S_0 to S_1 transition. The Mn_4CaO_5 cluster has a chain of strongly H-bonded 8 water molecules (O4-water chain) directly linked to O4 (linking Mn4 and Mn3 in the Mn_3CaO_4-cubane) and the release of the proton occurs along the O4-water chain in the S_0 to S_1 transition[3–5]. In S_0 and S_1[6], the ligand water molecules W1–W4 are H_2O in quantum mechanical/molecular mechanical (QM/MM) models (i.e., in the presence of the PSII protein environment)[3,7,8], whereas W2 is assumed to be OH^- in simplified QM models (i.e., in the absence of the PSII protein environment)[9–11]. The release of the proton is also observed in the S_2 to S_3 transition. Based on the observations of the recent radiation-damage-free structures obtained using the X-ray free electron laser (XFEL), the sixth O site, O6, may be incorporated into the Mn1 and O5 moieties of the Mn_4CaO_5cluster in the S_2 to S_3 transition[12–14].

During the water incorporation process, deprotonation of the water molecule may occur as proposed (e.g., water incorporation into the Mn1 moiety[15,16], water incorporation from the Ca^{2+} moiety[17–19]). In theoretical models by Shoji et al.[17] and Isobe et al.[20], it was assumed the presence of OH^- at W2 in S_2 to facilitate the release of the proton from H_2O at W3 to OH^- at W2, and proposed that deprotonation of W3 at the Ca^{2+} moiety occurs in the S_2 to S_3 transition. If OH^- needed to be located at either W2 or W3, placing OH^- at W2 and H_2O at W3 would be consistent with the experimentally measured values, $pK_a(Ca^{2+}) = 12.8 >> pK_a(Mn^{3+}) = 0.7$[21] in water. In theoretical models by Ames et al.[22], Rapatskiy et al.[23], Pérez-Navarro et al.[24], and Capone et al.[25], W2 was also assumed to be OH^-.

If the Mn_4CaO_5 cluster were isolated from the protein environment, placing OH^- at W2, not at W3, might be explained by $pK_a(Ca^{2+}) >> pK_a(Mn^{3+})$. However, placing OH^- at W2 is not consistent with the PSII crystal structures. The PSII crystal structures show that W2 has no strong H-bond acceptor, whereas W1 has a strong H-bond acceptor, D1-Asp61. Quantum mechanical/ molecular mechanical calculations show that H_2O at W1 forms a low-barrier H-bond with D1-Asp61 and is ready for proton transfer in S_2[26]. This may correspond to the significant changes in the H-bond properties between D1-Asp61 and a water molecule in the S_1 to S_2 transition observed in Fourier transform infrared (FTIR) spectroscopy[27]. Consistently, FTIR spectra suggested that W2 is H_2O in S_1 and S_2[8].

As far as we are aware, the pK_a values of the four water molecules at the Mn_4CaO_5 moiety, even those for the ligand water molecules W1–W4 are not reported. Robertazzi et al. reported that in S_1, $pK_a(W2) = 6.1$ for the isolated Mn_4CaO_5 cluster with deprotonated D1-His337 and 7.8 for the isolated Mn_4CaO_5 cluster with protonated D1-His337 in water, based on quantum chemical calculations[28]. However, the pK_a values for W1, W3, and W4 are not reported, which prevent from identifying the deprotonation sites even in the isolated Mn_4CaO_5 cluster in water. It should also be noted that the definition of the Mn_4CaO_5 cluster is vague. It can be comprised of Mn_4CaO_5, four ligand water molecules (W1–W4), and seven ligand residues (D1-Asp170, D1-Glu189, D1-His332, D1-Glu333, D1-Asp342, D1-Ala344, and CP43-Glu354, Fig. 1). It can also include the second sphere ligand residues, D1-Asp61, and CP43-Arg357, or the O4-water chain that forms an H-bond with O4. D1-Asp61 serves as an H-bond acceptor for W1 and is likely to facilitate proton transfer in the S_2 to S_3 transition[26]. The O4-water chain forms a significantly short H-bond with O4 (O…O < 2.5 Å) in the crystal structures in S_1 (or a slightly lower S-state)[29,30] and facilitates the release of the proton from O4 in the S_0 to S_1 transition[3–5]. The involvement of these proton acceptor groups (i.e., proton transfer pathways) facilitates deprotonation of the H-bond donor sites of the Mn_4CaO_5 cluster and decreases the pK_a values. This fact already implies that the pK_a values of the isolated Mn_4CaO_5 cluster in water are far from the relevant pK_a values in the PSII protein environment.

Here we report the pK_a values of the W1–W4 sites in the isolated Mn_4CaO_5 cluster in water, using quantum chemical approaches. To investigate the energetics of release of the proton towards the proton-transfer pathways in PSII, we analyze the potential-energy profiles of the H-bonds between the ligand water molecules and the H-bond acceptor (i.e., the proton acceptor) groups in the PSII protein environment. The results show that $pK_a(W1) \approx pK_a(W2) << pK_a(W3) \approx pK_a(W4)$ in the Mn_4CaO_5 cluster in water (i.e., in the absence of the PSII protein environment), whereas $pK_a(W1) \approx pK_a(D1\text{-}Asp61) << pK_a(W2)$ in PSII.

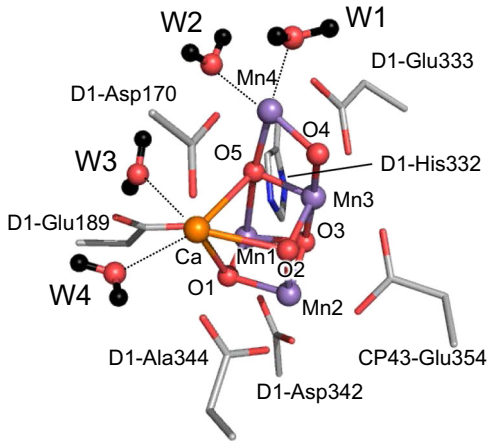

Fig. 1 Structure of the Mn_4CaO_5 cluster. The second sphere ligand residues (D1-Asp61 and CP43-Arg357) are not shown. Dotted lines indicate ligations of the ligand water molecules to the Mn4 and Ca^{2+} sites.

Results and discussion

We calculate the energy difference (ΔE_{water}) between the protonated and deprotonated states of hexa-aqua metal complexes in water (Fig. 2). The calculated ΔE_{water} values of hexa-aqua metal complexes with the valences of II, III, and IV show a correlation with the experimentally measured pK_a values (Fig. 3) and are best fitted to the following equation:

$$pK_a = 0.220\,\Delta E_{water}[\mathrm{kcal/mol}] - 55.8 \quad (1)$$

The calculated pK_a values of hexa-aqua metal complexes obtained using Eq. 1 are listed in Table 1. Note that in vacuum, the experimentally measured pK_a values cannot be reproduced using a single equation (Supplementary Fig. 1, Supplementary Table 1), because the electrostatic influence between the cationic metal and anionic OH^- in the deprotonated state is overestimated in vacuum. Thus, pK_a predominantly depends on the metal valence in vacuum.

The isolated Mn_4CaO_5 cluster is comprised of Mn_4CaO_5, four ligand water molecules (W1–W4), and seven ligand residues (D1-

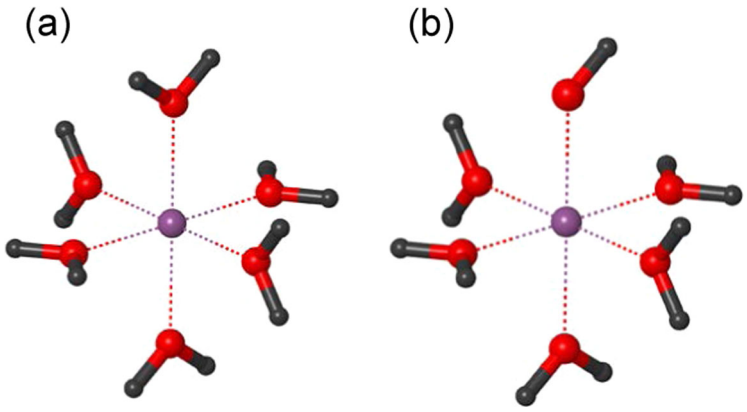

Fig. 2 Structures of hexa-aqua metal complexes. a Protonated state. **b** Deprotonated state. Magenta balls indicate metal ions. Dotted lines indicate ligations of the ligand water molecules to metal ions.

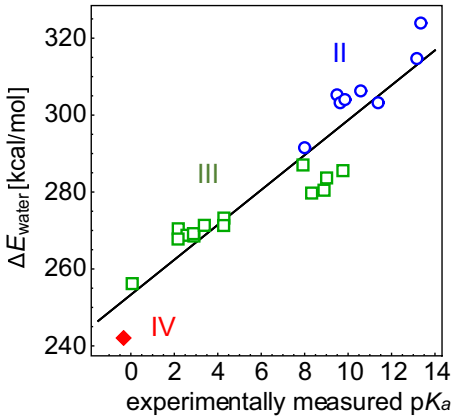

Fig. 3 Experimentally measured pK_a values and calculated H_2O/OH^- energy differences of hexa-aqua metal complexes. Blue open circles for divalent (II) metals, green open squares for trivalent (III) metals, and red closed diamond for the tetravalent (IV) metal.

Table 1 Calculated (Calc.) and experimentally measured (Expl.) pK_a of hexa-aqua metal complexes.

Metal ion	Calc. pK_a	Expl. pK_a
Zr^{4+}	−2.6	−0.32[a]
Mn^{3+} (high spin)	0.5	0.08[b]
Fe^{3+} (high spin)	3.1	2.19[b]
Ti^{3+}	3.7	2.20[b]
V^{3+}	3.3	2.60[b]
Ru^{3+} (low spin)	3.4	2.90[b]
Co^{3+} (low spin)	3.3	2.92[b]
Rh^{3+} (low spin)	3.9	3.40[b]
Cr^{3+}	3.9	4.29[b]
Sc^{3+}	4.3	4.30[b]
Lu^{3+}	5.7	7.94[a]
Cu^{2+}	10.9	8.0[b]
Y^{3+}	7.0	8.34[a]
Pr^{3+}	5.9	8.91[a]
La^{3+}	7.3	9.03[a]
Fe^{2+} (high spin)	11.3	9.50[b]
Co^{2+} (high spin)	10.9	9.65[b]
Gd^{3+}	6.6	9.78[a]
Ni^{2+}	11.1	9.86[b]
Mn^{2+} (high spin)	11.6	10.59[b]
Mg^{2+}	8.3	11.41[a]
Sr^{2+}	13.4	13.18[a]
Ba^{2+}	15.5	13.36[a]
RMSD[c]	1.5	

[a]Ref. 21.
[b]Ref. 34.
[c]Root mean square deviation (RMSD) of the calculated pK_a values from the experimentally measured pK_a values.
Calc. pK_a is obtained using Eq. (1).

Asp170, D1-Glu189, D1-His332, D1-Glu333, D1-Asp342, D1-Ala344, and CP43-Glu354, Fig. 1). Using Eq. (1), the pK_a values for W1–W4 are calculated at the isolated Mn_4CaO_5 cluster in water (in the absence of the PSII protein environment, Fig. 1). pK_a(W1) and pK_a(W2) on the dangling Mn4 site are 7–11, whereas pK_a(W3) and pK_a(W4) on Ca^{2+} site are 14–18 (Table 2). pK_a(W1) and pK_a(W2) are higher than pK_a of 0.5 for Mn^{3+} (Table 1), because Mn4 has two ligand acidic residues, D1-Asp170 and D1-Glu333, and two μ-oxo O atoms, O4 and O5 (Fig. 1). The difference in the pK_a of >5 between the Mn4 and Ca^{2+} sites (Table 2) indicate that the Ca^{2+} site is originally disadvantageous for H_2O deprotonation with respect to the Mn4 site. In particular in the PSII protein environment, W1 at Mn4 has D1-Asp61 as an H-bond acceptor, whereas W3 and W4 at Ca^{2+} do not have the corresponding acidic residues (see below). Thus, deprotonation of H_2O and incorporation of the generated OH^- into the Mn_4CaO_5 cluster occurring at the Ca^{2+} moiety in the S_2 to S_3 transition (e.g., refs. [17–19]) needs to overcome the energetic disadvantage.

As far as the ligand coordination in the PSII protein structure is maintained (i.e., the torsion angles are fixed), pK_a(W2) is only marginally (~1 pK_a unit) lower than pK_a(W1) in the absence of the PSII protein environment (Table 2). When the geometry is fully relaxed (i.e., the torsion angles are not fixed) and OH^- is initially placed at W4 [to calculate pK_a(W4)], proton transfer occurs from W2 via W3 to W4 occurs and OH^- is finally stabilized at W2, not at W1 (Supplementary Fig. 2). Deprotonation of W2 instead of W1 is just an artifact as W2, W3, and W4 form the H-bond network, pushing W1 and W3 away from Mn4 and Ca^{2+}, respectively (W1...Mn4 = 3.8 Å and W3...Ca^{2+} = 3.6 Å). These observations may be a basis of why electron paramagnetic resonance (EPR) signals were often interpreted based on theoretical models, in which W2 was assumed to be OH^- in QM-based models (i.e., in the absence of the PSII protein environment, e.g., refs. [10,22,23]). Interestingly, W2 = OH^- are also assumed in other QM-based models (e.g., by Siegbahn[9] and Retegan et al.[11]), without using QM/MM approaches. It should be noted that W2, W3, and W4 never form the H-bond network as far as the PSII protein environment exists.

The marginally low pK_a(W2) with respect to pK_a(W1) (Table 2) were the case only when the Mn_4CaO_5 cluster could be ideally isolated from the PSII protein environment. In such a model

system, pK_a(W1) and pK_a(W2) can change easily, depending on even the definition of the Mn_4CaO_5 cluster. When the second sphere ligand residues (D1-Asp61 and CP43-Arg357) are included in the model system of the Mn_4CaO_5 cluster in water, H_2O at W1 is not stable, releasing the proton, and is stabilized as OH^- at W1 in the presence of protonated D1-Asp61 (Fig. 4a), i.e., pK_a(W1) << pK_a(W2) (Table 3). The absence of the corresponding acidic residue as an H-bond acceptor for W2 and the proceeding proton transfer pathway (e.g., the D1-Asp61 pathway for W1[26]) contribute to an increase in pK_a(W2) with respect to pK_a(W1).

In the isolated Mn_4CaO_5 cluster in water (in the absence of the PSII protein environment), proton release occurs along the transiently formed H-bond between the ligand water molecule and a bulk water molecule (i.e., mobile water molecule with a high dielectric constant ≈ 80). The acceptor water molecule is best represented implicitly using the polarizable continuum model (PCM) method; in this case, the pK_a value of the deprotonation site of the Mn_4CaO_5 cluster can be calculated, whereas the pK_a difference between the deprotonation site and the adjacent proton-acceptor water molecule cannot be calculated directly. On the other hand, in the presence of the PSII protein environment, proton release occurs along the H-bond between the ligand water molecule and the fixed acceptor group (i.e., fixed dipole with a low dielectric constant << 80) (Fig. 4b). The acceptor group is represented explicitly based on the crystal structure; in this case, the energy barrier, which is associated with the pK_a difference between the deprotonation site and the acceptor group[31], can be calculated based on the potential-energy profile of the H-bond, whereas the pK_a value of the deprotonation site of the Mn_4CaO_5 cluster cannot be calculated directly. Note that only when the acceptor groups are always the same for all deprotonation sites (e.g., H_2O), the pK_a values may be calculated from the pK_a difference [e.g., the difference from pK_a(H_2O/H_3O^+)][31]. However, this is not the case for W1–W4 in the PSII protein environment, where the individual explicit acceptor groups already exist (e.g., D1-Asp61 for W1 and W446 for W2).

QM/MM calculations show that H_2O at W1 forms a low-barrier H-bond with D1-Asp61 and the proton migrates towards the D1-Asp61 moiety in S_2 (Fig. 5a), whereas H_2O at W2 forms a standard H-bond with an adjacent water molecule (W446, Fig. 4b) and the proton is localized at the W2 moiety, i.e., proton transfer from W2 to the acceptor H_2O is energetically uphill (Fig. 5b). This suggests that pK_a(W1) is significantly lower than pK_a(W2) in the PSII protein electrostatic environment and W2 cannot release the proton as more deprotonatable W1 exists at the Mn_4CaO_5 moiety in the PSII protein environment[32]. The results are consistent with W2

Table 2 pK_a of the Mn_4CaO_5 cluster in water. Supplementary Table 2 for anti-ferromagnetic spin configuration.

S state	Mn1, Mn2, Mn3, Mn4[a]	W1	W2	W3	W4
S_0	III, IV, III, III	11.3	10.1	17.7	16.4
S_0 [O4-H][b]	III, IV, III, III	9.5	9.0	16.6	16.0
S_0 [O5-H][c]	III, IV, III, III	10.0	8.5	16.1	15.4
S_1	III, IV, IV, III	10.2	9.0	15.6	15.1
S_2 [open][d]	III, IV, IV, IV	8.3	8.2	15.6	15.9
S_2 [closed][e]	IV, IV, IV, III	9.7	7.1	14.2	15.6

[a]Ferromagnetic spin configuration.
[b]O4 is protonated.
[c]O5 is protonated.
[d]Open-cubane structure.
[e]Closed-cubane structure.

Table 3 pK_a of the Mn_4CaO_5 cluster with D1-Asp61 and CP43-Arg357 in water.

S state	Mn1,Mn2,Mn3,Mn4[a]	W1	W2	W3	W4
S_0	III, IV, III, III	<<pK_a(W2)[f]	10.6	17.4	15.7
S_0 [O4H][b]	III, IV, III, III	<<pK_a(W2)[f]	9.6	15.5	14.8
S_0 [O5H][c]	III, IV, III, III	<<pK_a(W2)[f]	8.8	14.9	14.7
S_1	III, IV, IV, III	<<pK_a(W2)[f]	10.2	16.6	13.6
S_2 [open][d]	III, IV, IV, IV	<<pK_a(W2)[f]	9.1	13.8	13.8
S_2 [closed][e]	IV, IV, IV, III	<<pK_a(W2)[f]	8.8	14.1	14.6

[a]Ferromagnetic spin configuration.
[b]O4 is protonated.
[c]O5 is protonated.
[d]Open-cubane structure.
[e]Closed-cubane structure.
[f]not determined because of deprotonation of W1 to D1-Asp61.

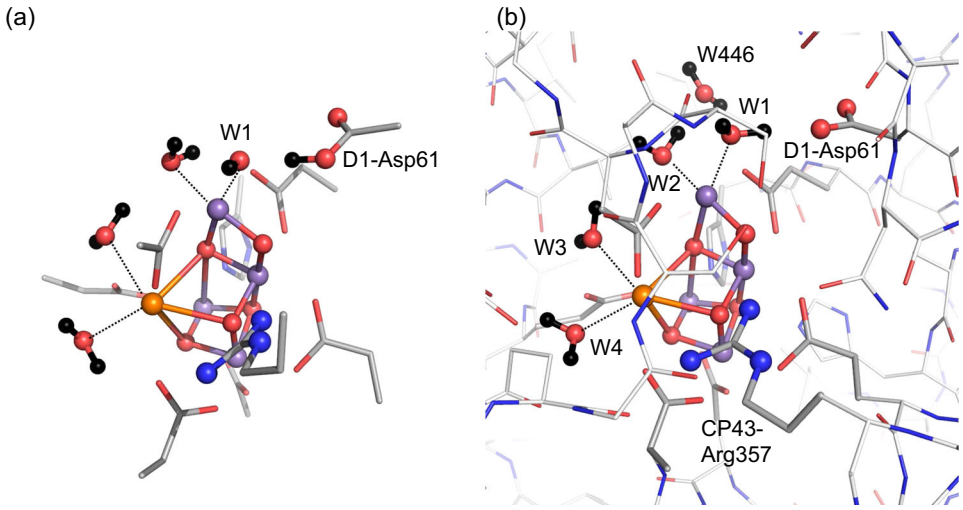

Fig. 4 Mn_4CaO_5 structures including the second sphere ligand residues (D1-Asp61 and CP43-Arg357) in S_1. Dotted lines indicate ligations of the ligand water molecules to metal ions. **a** Quantum-chemically optimized structure in the absence of the PSII protein environment. W1 is stabilized as OH^- in the presence of protonated D1-Asp61, as the release of the proton occurs from H_2O at W1 to ionized D1-Asp61. **b** QM/MM-optimized Mn_4CaO_5 structure in the PSII protein environment.

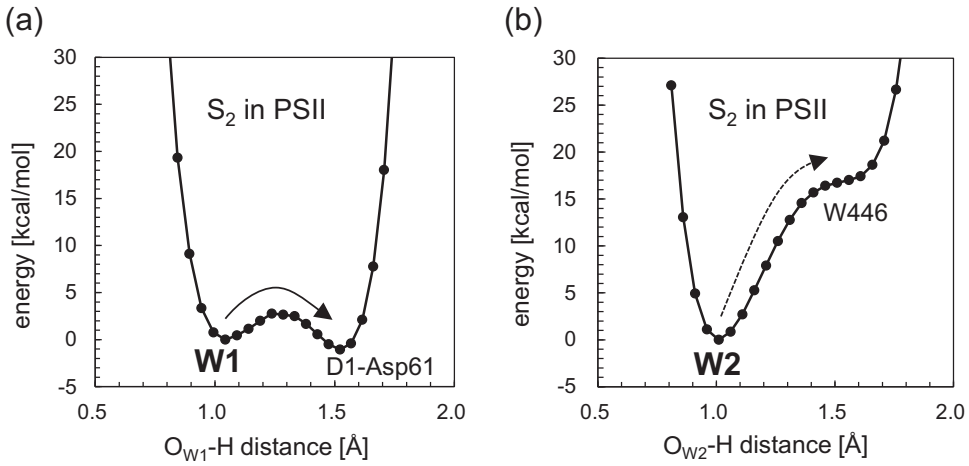

Fig. 5 The potential energy profiles of the H-bonds in S_2 [(Mn1, Mn2, Mn3, Mn4) = (III, IV, IV, IV)] in the PSII protein environment. a W1 and D1-Asp61. The isoenergetic proton transfer from W1 to D1-Asp61 indicates that pK_a(W1) ≈ pK_a(D1-Asp61). **b** W2 and the H-bond acceptor water molecule, W446. The energetically uphill proton transfer from W2 to W446 indicates pK_a(W2) >> pK_a(W1), i.e., deproton$_a$tion of W2 is energetically less favorable than deprotonation of W1.

being H_2O in S_1 and S_2 based on FTIR spectra and theoretical calculations by Nakamura and Noguchi[8].

In summary, pK_a(W1) ≈ pK_a(W2) << pK_a(W3) ≈ pK_a(W4) in the Mn_4CaO_5 cluster in water (Table 2). pK_a(W2) is only marginally (~1 pK_a unit) lower than pK_a(W1) in the absence of the PSII protein environment (Table 2) if the Mn_4CaO_5 cluster is defined as shown in Fig. 1, which may be a basis of why electron paramagnetic resonance (EPR) signals were often interpreted based on simplified theoretical models with OH^- at W2 (e.g., refs. [10,22,23]). pK_a(W1) is significantly lower than pK_a(W2) if the Mn_4CaO_5 cluster includes the second sphere ligand residues, D1-Asp61 and CP43-Arg357 (Table 3, Fig. 4a). Thus, as pK_a(W1) and pK_a(W2) depend strongly on the definition of the Mn_4CaO_5 region, pK_a(W1) and pK_a(W2) in water (in the absence of the protein environment) do not provide any clue to understanding the deprotonation sites in the physiological S-state transitions. The potential energy profiles of the H-bonds show that in the presence of the PSII protein environment in S_2 Fig. 4b), H_2O at W1 forms a low-barrier H-bond with D1-Asp61 and proton transfer is barrier-less (Fig. 5a)[26], whereas H_2O at W2 forms a standard H-bond with the adjacent H_2O and proton transfer is energetically uphill (Fig. 5b)[32]. These suggest that pK_a(W1) ≈ pK_a(D1-Asp61) << pK_a(W2) in PSII. As far as W1 exists, W2 can never release the proton (i.e., not OH^-) in PSII.

Methods

pK_a calculation. In the deprotonation reaction of the protonated state (AH) to deprotonated state (A^-) in water, pK_a is defined as

$$pK_a = \frac{\Delta G_{water}}{2.303\,RT}, \quad (2)$$

where ΔG_{aq} is the free energy difference between (AH) and ($A^- + H^+$) (i.e., $\Delta G_{water} = G_{water}(A^-) - G_{water}(AH) + G_{water}(H^+)$), R is the gas constant, and T is the temperature. ΔG_{water} can also be approximated as

$$\Delta G_{water} = k\Delta E_{water} + C, \quad (3)$$

where k is the scaling factor, ΔE_{water} is the energy difference between AH and A^-, which can be calculated using a quantum chemical approach with the PCM method, and C is the constant (simple pK_a estimation with energy of the optimized geometry scheme[33]). If the pK_a values of molecules are obtained at the same temperature, Eq. (2) can be written into Eq. (4) using the Eq. (3) as

$$pK_a = k'\Delta E_{water} + C', \quad (4)$$

where k' is the scaling factor and C' is constant. To determine k' and C', we calculated ΔE_{water} for 23 hexa-aqua metal complexes whose experimentally measured pK_a values are reported[21,34].

Hexa-aqua metal complex. The optimized geometry of the protonated hexa-aqua metal complex was obtained, using the restricted or unrestricted density functional theory with the B3LYP functional. The CSDZ* basis set was used for lanthanides except for La, the ERMLER2* basis set for actinides, and the LACVP* basis set for all other atoms. The spin states were consistent with previous studies by Galstyan et al.[34]. The optimized geometries of the deprotonated hexa-aqua metal complexes were obtained, fixing the torsion angles to prevent OH^- from forming an H-bond with other ligand H_2O molecules. However, the H-bond formation between the ligand OH^- and H_2O molecules could not be avoided for Ca^{2+}, Zn^{2+}, Cd^{2+}, Dy^{3+}, Th^{4+}, Pa^{4+}, U^{4+}, Np^{4+}, and Pu^{4+}, which were excluded from the present study. It should be noted that by adding a few external H_2O molecules to the ligand OH^- moiety, the H-bond formation between the ligand OH^- and H_2O molecules could be avoided without fixing the torsion angles. It was reported that the pK_a values for hexa-aqua metal complexes in water did not differ significantly when calculated by fixing the torsion angles or adding a few external H_2O molecules[34], probably because the shape of the hexa-aqua metal complex is symmetrical. However, this does not hold true for W1–W4 in the Mn_4CaO_5 cluster whose shape is not symmetric. Adding a few external H_2O molecules to the ligand OH^- moiety causes structural changes with respect to the original coordination geometry of the PSII crystal structure. In addition, explicit H_2O water molecules (i.e., fixed dipole) form a specific H_2O cluster (i.e., the dielectric constant << 80) at the deprotonatable ligand moiety, which does neither represent bulk water (i.e., the dielectric constant ≈ 80) nor provide the relevant pK_a values. Based on these, the torsion angles were fixed to obtain the optimized geometry for pK_a calculations in the present study. Using the optimized geometries, the energy difference (ΔE_{water}) between the protonated and deprotonated states of hexa-aqua metal complexes were calculated with PCM method, using the Jaguar program[35].

Mn_4CaO_5 cluster. The optimized geometry of the Mn_4CaO_5 cluster in the PSII protein environment was obtained as follows: the atomic coordinates of PSII were taken from the X-ray structure of PSII monomer unit "A" of the PSII complexes from *Thermosynechococcus vulcanus* at a resolution of 1.9 Å (PDB code, 3ARC)[29]. Atomic partial charges of the amino acids were adopted from the all-atom CHARMM22[36] parameter set, respectively. D1-His337 was considered to be protonated[8]. We employed the electrostatic embedding QM/MM scheme, in which electrostatic and steric effects created by a protein environment were explicitly considered, and we used the Qsite[37] program code. We employed the unrestricted DFT method with the B3LYP functional and LACVP* basis sets. To analyze the Mn_4CaO_5 geometries and the H-bond potential-energy profiles, the QM region was defined as the Mn_4CaO_5 cluster (including the ligand side-chains of D1-Asp170, D1-Glu189, D1-His332, D1-Glu333, D1-Asp342, CP43-Glu354, the ligand carboxy-terminal group of D1-Ala344, and the ligand water molecules, W1–W4), the Cl-1 binding site (Cl-1, W442, W446, and the side-chains of D1-Asn181 and D2-Lys317), and the second-sphere ligands (side-chains of D1-Asp61 and CP43-Arg357). Specifically, the coordinates of the heavy atoms in the surrounding MM region were fixed at their original X-ray coordinates, while those of the H atoms in the MM region were optimized using the OPLS2005 force field. All of the atomic coordinates in the QM region were fully relaxed (i.e., not fixed) in the QM/MM calculation. All of the H-bond partners were included in the QM region. The cluster was considered to comprise ferromagnetically coupled Mn atoms, where the total spin $S = 15/2$ in S_0, 14/2 in S_1, and 13/2 in S_2. The resulting Mn oxidation states (Mn1, Mn2, Mn3, Mn4) were (III, IV, III, III) in S_0, (III, IV, IV, III) in S_1, (III, IV, IV, IV) in open-cubane S_2, and (IV, IV, IV, III) in closed-cubane S_2. It should be noted that the difference in S (e.g., $S = 1/2$ in S_2[38], high,

low, ferromagnetic, and antiferromagnetic) did not affect the values; e.g., (i) the resulting geometry[39,40], (ii) the potential energy profile of proton transfer[26], (iii) the redox potential of each Mn site[41], and (iv) the pK_a values for the ligand water molecules W1–W4 in the absence of the protein environment (see Supplementary Table 2). To obtain the potential energy profiles of the O…H^+…O bond, the QM/MM optimized geometry was used as the initial geometry. The H atom under investigation was moved between the two O moieties by 0.05 Å, after which the geometry was optimized by constraining the distance between O–H^+ and H^+–O distances, and the energy was calculated. This procedure was repeated until the H atom reached the O moieties.

In the absence of the PSII protein environment (i.e., in vacuum), the QM/MM-optimized geometry was re-optimized, using the unrestricted density functional theory with the B3LYP functional and LACVP* basis sets and fixing the torsion angles to maintain the overall shape of the less stable complex. The QM region was defined as either the Mn_4CaO_5 cluster (including the ligand side-chains of D1-Asp170, D1-Glu189, D1-His332, D1-Glu333, D1-Asp342, CP43-Glu354, the ligand carboxy-terminal group of D1-Ala344, and the ligand water molecules, W1–W4) or the Mn_4CaO_5 cluster and the second-sphere ligands (side-chains of D1-Asp61 and CP43-Arg357). Using the optimized geometries, the energy difference (ΔE_{water}) between the protonated and deprotonated states of the Mn_4CaO_5 cluster were calculated with the PCM method, using the Jaguar program[35].

Data availability

All data generated or analyzed during this study are included in this article (and its Supplementary Information files).

Received: 10 April 2020; Accepted: 30 June 2020;
Published online: 16 July 2020

References

1. Shen, J. R. The structure of photosystem II and the mechanism of water oxidation in photosynthesis. *Annu. Rev. Plant. Biol.* **66**, 23–48 (2015).
2. Cardona, T. & Rutherford, A. W. Evolution of photochemical reaction centres: more twists? *Trends Plant Sci.* **24**, 1008–1021 (2019).
3. Saito, K., Rutherford, A. W. & Ishikita, H. Energetics of proton release on the first oxidation step in the water-oxidizing enzyme. *Nat. Commun.* **6**, 8488 (2015).
4. Takaoka, T., Sakashita, N., Saito, K. & Ishikita, H. pK_a of a proton-conducting water chain in photosystem II. *J. Phys. Chem. Lett.* **7**, 1925–1932 (2016).
5. Shimizu, T., Sugiura, M. & Noguchi, T. Mechanism of proton-coupled electron transfer in the S_0-to-S_1 transition of photosynthetic water oxidation as revealed by time-resolved infrared spectroscopy. *J. Phys. Chem. B* **122**, 9460–9470 (2018).
6. Pantazis, D. A. Missing pieces in the puzzle of biological water oxidation. *ACS Catal.* **8**, 9477–9507 (2018).
7. Pal, R. et al. S-state model of the oxygen-evolving complex of photosystem II. *Biochemistry* **52**, 7703–7706 (2013).
8. Nakamura, S. & Noguchi, T. Infrared determination of the protonation state of a key histidine residue in the photosynthetic water oxidizing center. *J. Am. Chem. Soc.* **139**, 9364–9375 (2017).
9. Siegbahn, P. E. Mechanisms for proton release during water oxidation in the S2 to S3 and S3 to S4 transitions in photosystem II. *Phys. Chem. Chem. Phys.* **14**, 4849–4856 (2012).
10. Krewald, V. et al. Metal oxidation states in biological water splitting. *Chem. Sci.* **6**, 1676–1695 (2015).
11. Retegan, M. et al. A five-coordinate Mn(IV) intermediate in biological water oxidation: spectroscopic signature and a pivot mechanism for water binding. *Chem. Sci.* **7**, 72–84 (2016).
12. Suga, M. et al. Light-induced structural changes and the site of O=O bond formation in PSII caught by XFEL. *Nature* **543**, 131–135 (2017).
13. Kern, J. et al. Structures of the intermediates of Kok's photosynthetic water oxidation clock. *Nature* **563**, 421–425 (2018).
14. Suga, M. et al. An oxyl/oxo mechanism for oxygen-oxygen coupling in PSII revealed by an x-ray free-electron laser. *Science* **366**, 334–338 (2019).
15. Siegbahn, P. E. Water oxidation mechanism in photosystem II, including oxidations, proton release pathways, O–O bond formation and O_2 release. *Biochim. Biophys. Acta* **1827**, 1003–1019 (2013).
16. Siegbahn, P. E. M. Computational investigations of S_3 structures related to a recent X-ray free electron laser study. *Chem. Phys. Lett.* **690**, 172–176 (2017).
17. Shoji, M., Isobe, H. & Yamaguchi, K. QM/MM study of the S_2 to S_3 transition reaction in the oxygen-evolving complex of photosystem II. *Chem. Phys. Lett.* **636**, 172–179 (2015).
18. Ugur, I., Rutherford, A. W. & Kaila, V. R. I. Redox-coupled substrate water reorganization in the active site of Photosystem II—the role of calcium in substrate water delivery. *Biochim. Biophys. Acta* **1857**, 740–748 (2016).
19. Kim, C. J. & Debus, R. J. Evidence from FTIR difference spectroscopy that a substrate H_2O molecule for O_2 formation in photosystem II is provided by the Ca ion of the catalytic Mn_4CaO_5 cluster. *Biochemistry* **56**, 2558–2570 (2017).
20. Isobe, H., Shoji, M., Shen, J.-R. & Yamaguchi, K. Strong coupling between the hydrogen bonding environment and redox chemistry during the S_2 to S_3 transition in the oxygen-evolving complex of photosystem II. *J. Phys. Chem. B* **119**, 13922–13933 (2015).
21. Dean, J.A. in *Lange's Handbook of Chemistry* (ed J. A. Dean) (McGraw-Hill Book Co, 1985).
22. Ames, W. et al. Theoretical evaluation of structural models of the S_2 state in the oxygen evolving complex of photosystem II: protonation states and magnetic interactions. *J. Am. Chem. Soc.* **133**, 19743–19757 (2011).
23. Rapatskiy, L. et al. Detection of the water-binding sites of the oxygen-evolving complex of photosystem II using W-band ^{17}O electron-electron double resonance-detected NMR spectroscopy. *J. Am. Chem. Soc.* **134**, 16619–16634 (2012).
24. Pérez Navarro, M. et al. Ammonia binding to the oxygen-evolving complex of photosystem II identifies the solvent-exchangeable oxygen bridge (μ-oxo) of the manganese tetramer. *Proc. Natl Acad. Sci. USA* **110**, 15561–15566 (2013).
25. Capone, M., Narzi, D., Bovi, D. & Guidoni, L. Mechanism of water delivery to the active site of photosystem II along the S_2 to S_3 transition. *J. Phys. Chem. Lett.* **7**, 592–596 (2016).
26. Kawashima, K., Takaoka, T., Kimura, H., Saito, K. & Ishikita, H. O_2 evolution and recovery of the water-oxidizing enzyme. *Nat. Commun.* **9**, 1247 (2018).
27. Debus, R. J. Evidence from FTIR difference spectroscopy that D1-Asp61 influences the water reactions of the oxygen-evolving Mn_4CaO_5 cluster of photosystem II. *Biochemistry* **53**, 2941–2955 (2014).
28. Robertazzi, A., Galstyan, A. & Knapp, E. W. Reprint of PSII Manganese Cluster: Protonation of W2, O5, O4 and His337 in the S1 state explored by combined quantum chemical and electrostatic energy computations. *Biochim. Biophys. Acta* **1837**, 1389–1394 (2014).
29. Umena, Y., Kawakami, K., Shen, J.-R. & Kamiya, N. Crystal structure of oxygen-evolving photosystem II at a resolution of 1.9 Å. *Nature* **473**, 55–60 (2011).
30. Suga, M. et al. Native structure of photosystem II at 1.95 Å resolution viewed by femtosecond X-ray pulses. *Nature* **517**, 99–103 (2015).
31. Ikeda, T., Saito, K., Hasegawa, R. & Ishikita, H. The existence of an isolated hydronium ion in the interior of proteins. *Angew. Chem. Int. Ed.* **56**, 9151–9154 (2017).
32. Saito, K., Mandal, M. & Ishikita, H. Energetics of ionized water molecules in the H-bond network near the Ca^{2+} and Cl^- binding sites in photosystem II. *Biochemistry*, doi: 10.1021/acs.biochem.0c00177 (2020).
33. Matsui, T., Baba, T., Kamiya, K. & Shigeta, Y. An accurate density functional theory based estimation of pK_a values of polar residues combined with experimental data: from amino acids to minimal proteins. *Phys. Chem. Chem. Phys.* **14**, 4181–4187 (2012).
34. Galstyan, G. & Knapp, E. W. Computing pK_A values of hexa-aqua transition metal complexes. *J. Comput Chem.* **36**, 69–78 (2015).
35. Jaguar. version 7.9, Schrödinger, LLC, New York, NY (2012).
36. MacKerell, A. D. Jr. et al. All-atom empirical potential for molecular modeling and dynamics studies of proteins. *J. Phys. Chem. B* **102**, 3586–3616 (1998).
37. QSite. version 5.8, Schrödinger, LLC, New York, NY (2012).
38. Zimmermann, J. L. & Rutherford, A. W. Electron paramagnetic resonance properties of the S_2 state of the oxygen-evolving complex of photosystem II. *Biochemistry* **25**, 4609–4615 (1986).
39. Ames, W. et al. Theoretical evaluation of structural models of the S_2 state in the oxygen evolving complex of photosystem II: protonation states and magnetic interactions. *J. Am. Chem. Soc.* **133**, 19743–19757 (2011).
40. Isobe, H. et al. Theoretical illumination of water-inserted structures of the $CaMn_4O_5$ cluster in the S_2 and S_3 states of oxygen-evolving complex of photosystem II: full geometry optimizations by B3LYP hybrid density functional. *Dalton Trans.* **41**, 13727–13740 (2012).
41. Mandal, M., Kawashima, K., Saito, K. & Ishikita, H. Redox potential of the oxygen-evolving complex in the electron transfer cascade of photosystem II. *J. Phys. Chem. Lett.* **11**, 249–255 (2020).

Acknowledgements

This research was supported by JST CREST (JPMJCR1656 to H.I.), JSPS KAKENHI (18H05155, 18H01937, 20H03217, and 20H05090 to H.I., 16H06560 and 18H01186 to K. S.), and the Interdisciplinary Computational Science Program in CCS, University of Tsukuba (K.S.).

Author contributions

H.I. designed research; K.S., M.N., and H.I. performed research; K.S., M.N., and H.I. analyzed data; and H.I. wrote the paper.

Competing interests
The authors declare no competing interests.

Additional information
Supplementary information is available for this paper at https://doi.org/10.1038/s42004-020-00336-7.

Correspondence and requests for materials should be addressed to H.I.

Reprints and permission information is available at http://www.nature.com/reprints

Publisher's note Springer Nature remains neutral with regard to jurisdictional claims in published maps and institutional affiliations.